International Journal of Applied Mechanics
Vol. 13, No. 10 (2021) 2150116 (26 pages)

DOI: 10.1142/S1758825121501167

World Scientific
www.worldscientific.com

Laboratory for Validation of Rolling-Resistance Models

M. L. Larsen*, J. Cesbron†, F. Anfosso-Lédée‡,
C. Ropert§, J. C. Dyre* and T. Hecksher*,¶

*IMFUFA, Dept. of Science and Environment
Roskilde University, Denmark

†Univ Gustave Eiffel, Cerema, UMRAE
F-44344 Bouguenais, France

‡Univ Gustave Eiffel, MAST-LAMES
F-44344 Bouguenais, France

§Univ Gustave Eiffel, AME-EASE, F-44344 Bouguenais, France
¶tihe@ruc.dk

Received 10 August 2021
Accepted 17 November 2021
Published 31 December 2021

In this paper, a versatile drum setup for measuring rolling resistance of small wheels is presented. The purpose is to provide a flexible setup for testing of models for rolling resistance under controlled circumstances. To demonstrate this, measurements of rolling resistance with a series of sandpapers of different grit sizes representing surface textures were carried out. The measurements show a clear increase in the rolling-resistance coefficient with increasing surface roughness, rolling speed and load. Numerical calculations in the time domain for a visco-elastic contact model run on equivalent surfaces agree with the trends found experimentally. We conclude that this approach to simplifying the experiment in order to obtain a high degree of control, accuracy and repeatability is useful for validating and testing models for calculating the rolling resistance for a given surface texture.

Keywords: Rolling resistance; contact mechanics; surface analysis; visco-elasticity.

1. Introduction

Any driving vehicle needs a continuous input of energy — in most cases in the form of fossil fuels — to overcome driving resistance. Driving resistance comes from many different sources, the more prominent being aerodynamic drag, friction in mechanical parts and rolling resistance [Andersen *et al.*, 2015]. In order to decrease the fuel consumption, these losses need to be minimized. Much has been done from manufacturer's side on improving the fuel economy of cars, to reduce the rolling resistance of tires, etc. From an infrastructural perspective, only the road is readily

¶Corresponding author.

available for optimization. Since the 1970's, it has become increasingly clear that surface texture and unevenness (macro and mega texture) of roads is a source of driving resistance [Willis *et al.*, 2015]. In recent years, the focus on reduction of the rolling resistance of roads has intensified due to climate changes demanding an investigation of all possibilities for reducing the man-made CO_2 emission [Andersen *et al.*, 2015].

Rolling resistance is caused by visco-elastic effects in the rolling object and in the surface on which it rolls. The rolling object (tire) and surface (pavement) deform by the load exerted: the surface deflects and the rolling object flattens out slightly in the contact patch. Deformation of visco-elastic materials is not entirely reversible and thus causes dissipation of energy in the form of heat. Consequently, losses occur both in the tire and in the pavement. The latter is often referred to as "structural rolling resistance" to distinguish it from the tire rolling resistance, that is limited to the losses in the tire only. Few direct measurements exist that determine the magnitude of structural rolling resistance, but this is believed to be negligible for passenger cars [Chupin *et al.*, 2013], while model studies estimate it to be a factor of 10–100 smaller than tire rolling resistance even for heavy traffic [Pouget *et al.*, 2012; Bazi *et al.*, 2018; Nielsen *et al.*, 2020].

The ISO standard ISO25280 [2018] for labeling tire rolling resistance consider tires running on a smooth steel surface. However, tire rolling resistance is increased when the surface is textured because the texture causes localized indentations in the rubber in addition to the overall deformation. Most work on the texture dependence of rolling resistance either takes the form of empirical correlations between texture and measured rolling resistance [Willis *et al.*, 2015; Andersen *et al.*, 2015] focusing on full-scale studies (actual car tires on real roads) [Sandberg *et al.*, 2011, 2015; Bergiers *et al.*, 2011; Zöller, 2014; Anfosso-Lédée *et al.*, 2016; Haider *et al.*, 2016; Ejsmont *et al.*, 2017; Vieira *et al.*, 2019] or pure model studies [Sharma *et al.*, 2020].

While this experimental approach is the most common, some studies have used different methods: Araújo *et al.* [2019] used a small indoor test rig where a pneumetic tire is driven in a circular motion on the floor; [Ejsmont and Owczarzak, 2019] used the bouncing motion of a dropped tire for evaluating energy loss from different surface textures; Mansura *et al.* [2018] utilized a packed indenters loading test to measure energy loss for different surface textures; and Riahi *et al.* [2020] used a Wehner/Schulze polishing machine with three rubber cones mounted on the rotary head to measure rolling resistance of road specimens. Lundberg *et al.* [2017] constructed a test rig for accurate measurements of contact forces and Kawakami *et al.* [2017] correlated contact pressure distribution between tire and pavement surfaces to evaluate the rolling resistance indirectly.

The crucial question in all of these studies is how to characterize a given surface texture in a way that gives a good prediction of rolling resistance. The standardized texture measure is Mean Profil Depth (MPD) [ISO13473, 2019], which is also used in most studies. However, some studies suggest that MPD is not sufficient for this

purpose [Pinnington, 2012; Goubert and Sandberg, 2018; Ejsmont and Sommer, 2021].

Early model studies of rolling resistance were based on simplified tire models in two dimensions and focused on steady-state rolling on a flat surface [Stutts and Soedel, 1992; Kim and Savkoor, 1997; Miège and Popov, 2005]. More sophisticated modeling of pneumatic tires considers tire structure and compounds in 3D, as well as thermo-mechanical considerations in the calculation of energy dissipation due to heat generation [Park *et al.*, 1997; Lin and Hwang, 2004; Narasimha Rao *et al.*, 2006].

Only little has been done to test model predictions against experimental results. Lopez [2010] and Boere *et al.* [2014] assessed rolling resistance as the sum of energy dissipation due to large steady-state tire deformations on a flat surface and energy dissipation originating from tire vibrations induced by road texture in a two-step finite element model. They found a correlation between the predicted rolling resistance and the Root Mean Square (RMS) texture depth when comparing to an experimental database. Similar results have been found by Hoever and Kropp [2015] for 19 conventional road surfaces from the same data base. Likewise, Mansura *et al.* [2018] found their numerical calculations of a multi-scale tire model on surface texture to be in qualitative agreement with measurements on different road structures.

It is difficult to critically test rolling resistance models with real-life measurements beyond such correlation findings, mainly because many variables are not experimentally controlled, e.g., temperature, surface texture, weather, etc. The parameters of any model would have to be adjusted to fit a given measurement. The validation of a parameterization should include a comparison of model predictions for a different set of conditions to real-life measurements. In most cases, such data sets do not exist.

Here we take the approach of simplifying the experimental setup as much as possible, focusing on isolating the key variables of interest. Instead of attempting to arrive at a complete model of the real-life rolling resistance, we argue as follows: Any future model must be based on robust input in the form of a reliable underlying mathematical model for the rolling resistance between a rubber and a surface with a given texture. How can one ensure that this mathematical model is reliable? The only way is to be able to test it in the laboratory, i.e., under controlled circumstances. The aim is the assessment of the part of tire rolling resistance originating from hysteretic energy dissipation at the contact interface reflecting visco-elastic properties of the tire material. The laboratory prototype developed in this work consists of a simplified drum rig with a small solid rubber wheel inside the drum. Using this setup, rolling resistance can be investigated under controlled circumstances for visco-elastic wheels, allowing for investigations and possible validation of any mathematical rolling-resistance model. The setup is designed specifically for testing the capability of models to predict the rolling resistance for a given surface texture. As a proof of concept, we present here a series of measurements of small

solid rubber wheels rolling on sandpapers of varying grit size. The surface texture of the sandpapers is characterized to enable a numerical study on equivalent surfaces. It is important to emphasize that these are merely tests of the fundamental idea, not an attempt to realistically model the resistance between a pneumatic tire and a real asphalt or concrete road.

2. Rolling-Resistance Experiment

This section describes the custom-built experimental setup, measurement principle, protocol and results.

2.1. *Construction and working principle of the test rig*

Figure 1 shows a photo and a schematic drawing of the setup. It consists of a drum with the test wheel running on its inside. The test wheel is rotated by the drum, which in turn is driven by a motor. The conventional configuration [ISO18164, 2005; ISO25280, 2018] runs the wheel (or tire) on the outside of the drum. However, for adding texture to the drum, it is more convenient to have the wheel and texture on the inside because the centrifugal forces arising when the drum rotates help keeping the texture in place on the drum. The drum has an inner diameter of 0.538 m and the test wheels have diameters of 0.125 m. The moderate physical size of the setup allows for easy control of load between surface and wheel, speed/rotation velocity, wheel type and surface textures.

The motor (component f on Fig. 1(b)) is mounted on a freely rotating drum shaft. The torque delivered by the motor to maintain a constant angular velocity of the drum is measured by the bending of a cantilever spring that supports the motor

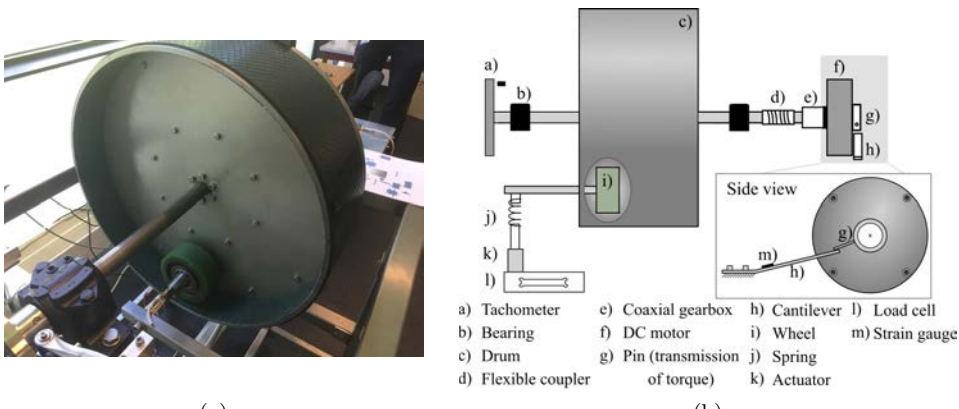

(a) (b)

Fig. 1. The drum setup. (a) Photo of the setup showing the inside of the drum with surface texture attached. (b) Schematic illustration of the drum setup showing how the different mechanical components are connected.

(components h on Fig. 1(b)), hindering its own opposite rotation. The torque needed to keep the drum at constant angular velocity balances the total resistance opposing the rotation, including friction in the bearings, air drag and rolling resistance. The bending of the cantilever spring is thus a direct measure of the resisting forces. The bending is measured by strain gauges and calibrated by weights. For more details, see Hansen and Larsen [2017].

The load on the wheel is controlled by an actuator connected via a spring to the wheel shaft. The actuator is mounted on a load cell that monitors the load continuously during the measurement (components j, k and l on Fig. 1(b)).

The measurement principle makes use of the balance of the torque for both the wheel and the drum. At constant angular velocity, there is no angular acceleration and thus $\sum \boldsymbol{\tau} = \mathbf{0}$, where τ is torque (notice that this is a vector sum). The sum of torques around the center of wheel is given by

$$\boldsymbol{\tau}^{\mathrm{O}}_{\mathrm{wheel}} = \boldsymbol{\tau}_{\mathrm{RR}} + \mathbf{r} \times \mathbf{F}_{\mathrm{drum}\to\mathrm{wheel}} + \boldsymbol{\tau}^{\mathrm{wheel}}_{\mathrm{loss}} = \mathbf{0} \tag{1}$$

where $\boldsymbol{\tau}_{RR}$ is the rolling resistance torque, $\mathbf{r} \times \mathbf{F}_{\mathrm{drum}\to\mathrm{wheel}}$ (see Fig. 2) is the torque deriving from the drum driving the rotation of the wheel, and $\boldsymbol{\tau}^{\mathrm{wheel}}_{\mathrm{loss}}$ is the torque coming from friction in the wheel bearing and air resistance.

The sum of torques around the center of the drum is likewise zero:

$$\boldsymbol{\tau}^{\mathrm{O'}}_{\mathrm{drum}} = \boldsymbol{\tau}_{\mathrm{motor}} + \mathbf{R} \times \mathbf{F}_{\mathrm{wheel}\to\mathrm{drum}} + \boldsymbol{\tau}^{\mathrm{drum}}_{\mathrm{loss}} = \mathbf{0} \tag{2}$$

where $\boldsymbol{\tau}_{\mathrm{motor}}$ is the torque delivered by the motor, i.e., what we measure, $\mathbf{R} \times \mathbf{F}_{\mathrm{wheel}\to\mathrm{drum}}$ is the torque opposing the rotation coming from the wheel, and $\boldsymbol{\tau}^{\mathrm{drum}}_{\mathrm{loss}}$ signifies the total torque due to friction, drag, etc. on the drum. The z-components of Eqs. (1) and (2) become

$$0 = -\tau_{RR} + rF_{\mathrm{drum}\to\mathrm{wheel}} - \tau^{\mathrm{wheel}}_{\mathrm{loss}} \tag{3}$$

$$0 = \tau_{\mathrm{motor}} - RF_{\mathrm{wheel}\to\mathrm{drum}} - \tau^{\mathrm{drum}}_{\mathrm{loss}} \tag{4}$$

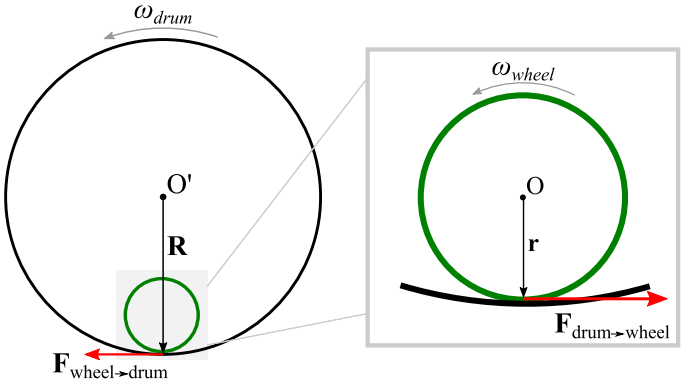

Fig. 2. Diagram showing drum and wheel. The torques relative to the center of the drum and wheel, respectively, sum to zero at constant angular velocity.

Due to the principle of action and reaction (Newton's third law), $\mathbf{F}_{\text{wheel}\to\text{drum}} = -\mathbf{F}_{\text{drum}\to\text{wheel}}$ (or equivalently for the magnitude $F_{\text{wheel}\to\text{drum}} = F_{\text{drum}\to\text{wheel}}$) we thus obtain

$$F_{\text{wheel}\to\text{drum}} = \frac{1}{r}(\tau_{RR} + \tau_{\text{loss}}^{\text{wheel}}) = \frac{1}{R}(\tau_{\text{motor}} - \tau_{\text{loss}}^{\text{drum}}) \tag{5}$$

which gives the following:

$$\tau_{\text{motor}} = \tau_{\text{loss}}^{\text{drum}} + \frac{R}{r}(\tau_{\text{RR}} + \tau_{\text{loss}}^{\text{wheel}}) \tag{6}$$

From "skim test reading" [ISO18164, 2005] we can determine the loss terms, i.e., the "parasitic losses". Skim test reading is a measurement where the wheel is positioned such that it just touches the drum surface and rotates without skidding and without deforming. In this position, one should have $\tau_{\text{RR}} = 0$, and thus $\tau_{\text{motor}}^{\text{skim test}} = \tau_{\text{loss}}^{\text{drum}} + \frac{R}{r}\tau_{\text{loss}}^{\text{wheel}}$. Consequently, the rolling-resistance force, F_{RR}, can be found by subtracting the skim test reading from the measurement with load as follows:

$$F_{\text{RR}} = \frac{\tau_{\text{RR}}}{r} = \frac{1}{R}(\tau_{\text{motor}} - \tau_{\text{motor}}^{\text{skim test}}) \tag{7}$$

where τ_{motor} is the measured quantity, both in the skim test reading and with load applied to the wheel. This procedure assumes that the loss in the various bearings in the setup is load-independent to a good approximation.

For the experiments presented in this paper, two solid rubber wheels (polyurethane rubber (PUR) and nitrile butadine rubber (NBR)) were used. Both wheels have a metal rim with the rubber attached and ball bearings in the center (see Fig. 3). The PUR wheel is a commercial pallet jack wheel that has an iron rim of 53 mm in radius with a PUR layer of 9 mm. The NBR wheel has an aluminium rim of radius 47 mm with a moulded layer of nitrile butadiene rubber of thickness 16 mm. Both wheels are 50 mm wide. Each wheel has its own set of bearings and can be easily exchanged by using the same spindle.

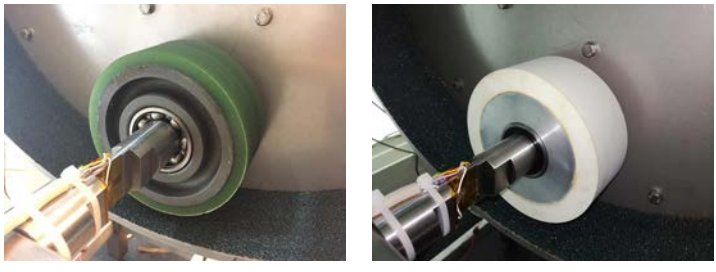

(a) (b)

Fig. 3. Photos of the two test wheels used in this study. (a) Commercial PUR pallet truck wheel. (b) Custom-made NBR wheel.

2.2. *Sandpapers and surface characterization*

The surface texture is varied by using sandpapers of different grit size. The sandpaper is cut to fit inside the drum and attached by thin double sided tape to the drum surface. Five different grit size sandpapers were used in addition to no sandpaper. Grit sizes of P400, P160, P60, P32 and P24 (according to the grit size standard FEPA) were used.

The profile heights of the different sandpapers were measured by a profilometer shown in Fig. 4(a). The sandpaper is placed below the profilometer on a flat floor. A laser sensor in the profilometer measures the distance from the sensor to the surface of the sandpaper. The position of the sensor is measured with an accuracy of 0.1 mm

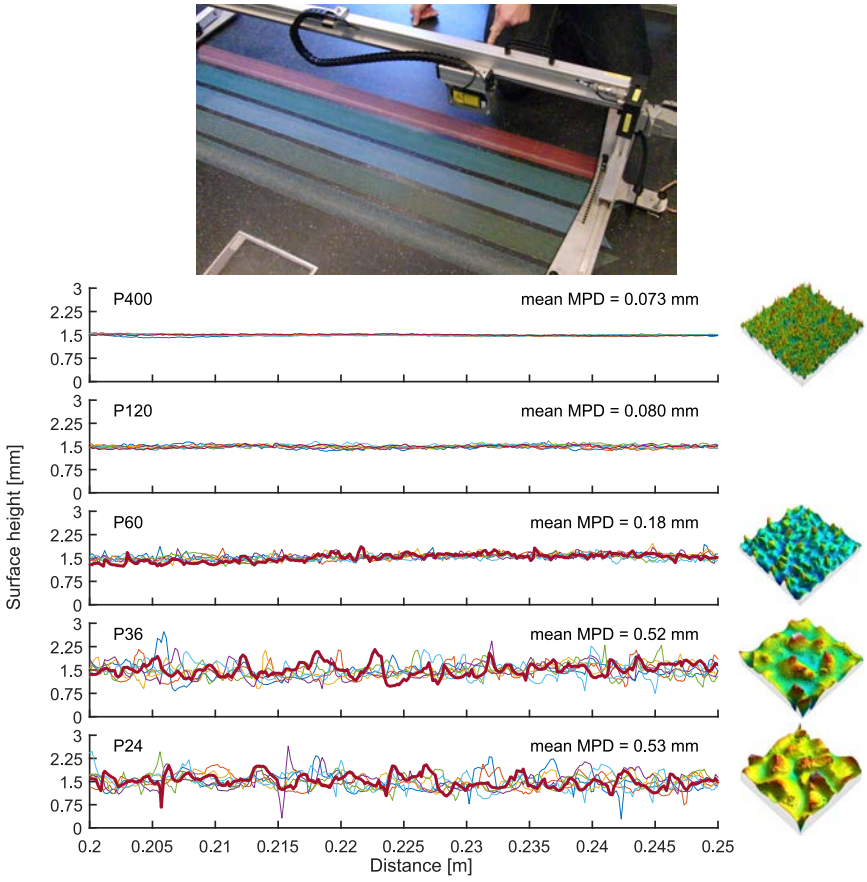

Fig. 4. Profile characterization of sandpapers used in the experiment. (a) Profilometer used to measure the surface profile of the five types of sandpaper. (b) Texture measurements for the following sandpapers: P400, P120, P60, P36 and P24. Each plot shows a section of the seven contour measurements over a length of 1.5 m. The MPD is calculated from the entire length of the seven contours. To the right of each contour plot (except for the P120 sandpaper) a high-resolution 3D height scan of a 4 mm×4 mm area is shown.

and the distance from the sensor to the surface is measured with an accuracy of 0.1 μm. A total of seven different paths were scanned for 1.5 m of each sandpaper type. Examples of the resulting curves are shown in Fig. 4(b). The Mean Profile Depth (MPD), a traditional indicator for road texture defined in ISO13473 [2019], was calculated on the basis of these profiles. Note that the MPD of the coarsest sandpaper (P24) is lower than that of the less coarse P36.

For P400, P60, P36 and P24 sandpapers, a detailed 3D height scan of 4 mm $\times$ 4 mm area is added in Fig. 4(b) to illustrate the difference in surface texture. These 3D scans of the surfaces were performed by the InfiniteFocus system from Alicona. The sensor is based on the technology of focus variation. It combines the shallow depth of field of an optical system with vertical scanning. The sample is placed on a motorized platform and illuminated by a white light which can be modulated. Coaxial light is provided by a semi-transparent mirror to a series of interchangeable lenses mounted on a six-position lens holder. The reflected light is returned through the semi-transparent mirror to a digital color sensor. The vertical and lateral resolutions can go up to 10 nm and 0.4 μm, respectively and are defined by the choice of the lens. In this study, a $\times 5$ magnitude was used, which led to a vertical resolution of 870 nm and lateral resolution of 7 μm. The image was similar to that of a microscope in the sense that it was limited by the depth of field. Images were acquired continuously while the sample to objective distance was changing. Each image varies with the distance and topography of the sample. It is critical to couple lighting, distance and image capture in this process. The focus quality is calculated for each position and its variation is used to determine the topography information.

For the contact model calculations detailed in Sec. 3, the 3D surface texture of sandpapers P24 and P60 were also measured by means of the same device. The spatial step of the measurement was $\Delta x = \Delta y = 0.007$ mm and $\Delta z = 1$ nm, respectively in the x-, y- and z-directions. The dimensions of the texture scan, namely 32.7 mm in the x-direction (rolling direction) and 83.6 mm in the y-direction, were limited by the capacity of the apparatus. Figure 5 shows the resulting 3D surface textures for sandpapers P24 and P60.

2.3. *Measurement protocol*

A measurement run is made for each combination of surface texture and wheel, giving a total of 2×6 measurement runs. Each run consists of a series of different target velocities and loads. Most of the runs for this work included two different velocities and five different loads, including a zero load measurement (the skim test reading), leading to a total of 10 different setting combinations. In addition, the last three measurement runs for each texture/wheel combination were conducted in order to ensure reproducibility.

The load is controlled by the position of the actuator and a measurement run starts by setting the actuator to the first position from the target values. Then

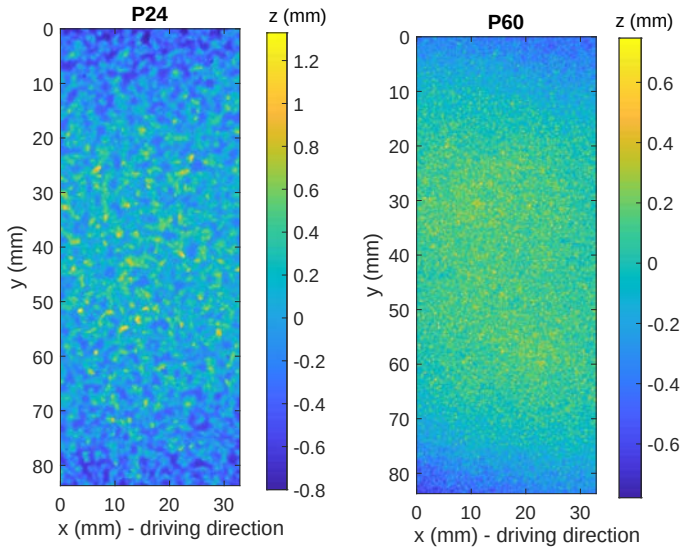

Fig. 5. Measured 3D surface textures used for contact calculation for sandpapers P24 (left) and P60 (right). The spatial resolution is $\Delta x = \Delta y = 0.007\,\text{mm}$.

the measurement program loops through the target velocities. The power to the motor is adjusted by a PID algorithm to reach the target rotational velocity of the drum. When the drum has maintained a stable rotational velocity for 30 min, the power to the motor is kept constant and the logging starts. After logging a fixed number of data points for averaging (taking usually roughly 30 min), the actuator is moved to the next target position in an increasing manner going from small to higher loads, iterating through the target velocities, until all target combinations have been measured. Each measurement run for this study took around 24 h.

Three quantities are monitored continuously during each measurement run: rotational velocity of the drum, the load on the wheel, and the torque exerted by the motor. An example of the output from one measurement run is shown in Fig. 6, illustrating the protocol. The gap between each target setting is the stabilization time.

2.3.1. *Calculating the rolling-resistance coefficient* μ_{RR}

The rolling-resistance coefficient is defined as the rolling-resistance force magnitude, F_{RR}, divided by the normal force magnitude, F_N

$$\mu_{\text{RR}} = \frac{F_{\text{RR}}}{F_N} \tag{8}$$

in analogy with the friction coefficient. The normal force balances the load and thus we can replace F_N by F_{load} when calculating the rolling-resistance coefficient from the measurements.

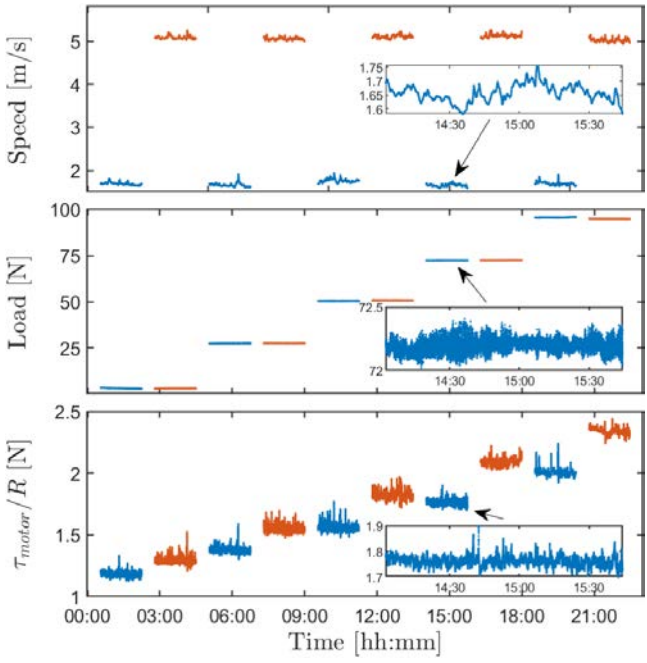

Fig. 6. Raw data from one measurement run with the NBR wheel on the steel surface illustrating the protocol. Each run starts at "zero" load, providing the skim test reading for determining the parasitic losses, then loops through the target velocities (here two), before changing to slightly higher load and repeating. Colors indicate measurements at different target velocities.

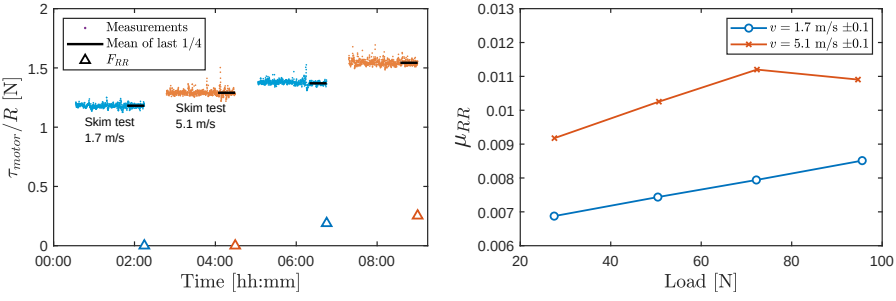

(a) (b)

Fig. 7. Determining the rolling-resistance coefficient. (a) Plot of the measured torque, showing how parasitic losses from skim test reading are subtracted. (b) Rolling-resistance coefficient as a function of load for the NBR wheel on a steel surface obtained from the data in (a).

In order to ensure a stabilized value, the load and resistance force are determined by averaging the last quarter of the data points for each setting. This procedure is illustrated for the resistance force in Fig. 7(a). The first actuator position of each measurement run is for the skim test reading. At this position only the parasitic

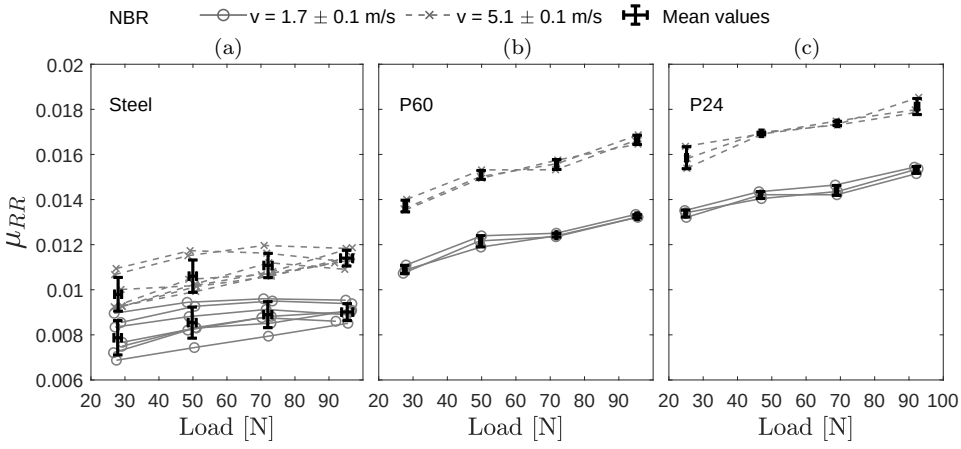

Fig. 8. Repeated measurements of the rolling-resistance coefficient as a function of load for NBR wheel.

losses, e.g., aerodynamic losses and losses from drum and wheel bearings, contribute to the total torque the motor must overcome. To obtain the rolling resistance deriving from a given surface, the skim test reading is subtracted from the measurements with non-zero load (Eq. (7)). Figure 7 shows how the average values for resistance for different speeds and loads change with and without parasitic losses. Figure 7(b) shows the μ_{RR} average values plotted as a function of the average load for the target position.

2.4. *Experimental results*

Figure 8 investigates the repeatability of the measurements. Rolling-resistance coefficients, μ_{RR}, for the NBR wheel run on the smooth steel, P60 and P24 textures, are shown as a function of load for the two velocities. The measurement runs are generally nicely repeatable, however slightly less so for the smooth steel surface than for the two textured surfaces. Despite the somewhat larger scatter in these results, the variations with load and speed are still clearly systematic.

In Figs. 9(a)–9(d), μ_{RR} is plotted as a function of load for all the different textures investigated and the two velocities. Data points represent the mean of three (in a few cases more) measurement runs and error bars give the standard deviations. Several trends can be observed in the data: (1) The NBR rolling resistance coefficients lie consistently above the PUR results for identical target settings. This reflects the different visco-elastic properties of the two materials. (2) There is a clear velocity dependence of μ_{RR} for the NBR wheel, while the PUR results are much less dependent of velocity. Again, this reflects different visco-elastic properties of the rubbers. Only two velocities were used for the main study, so a single measurement run was added for the NBR wheel looping through more velocities (shown in Fig. 9(e)), confirming the trend. (3) For both wheels there is an increase in rolling

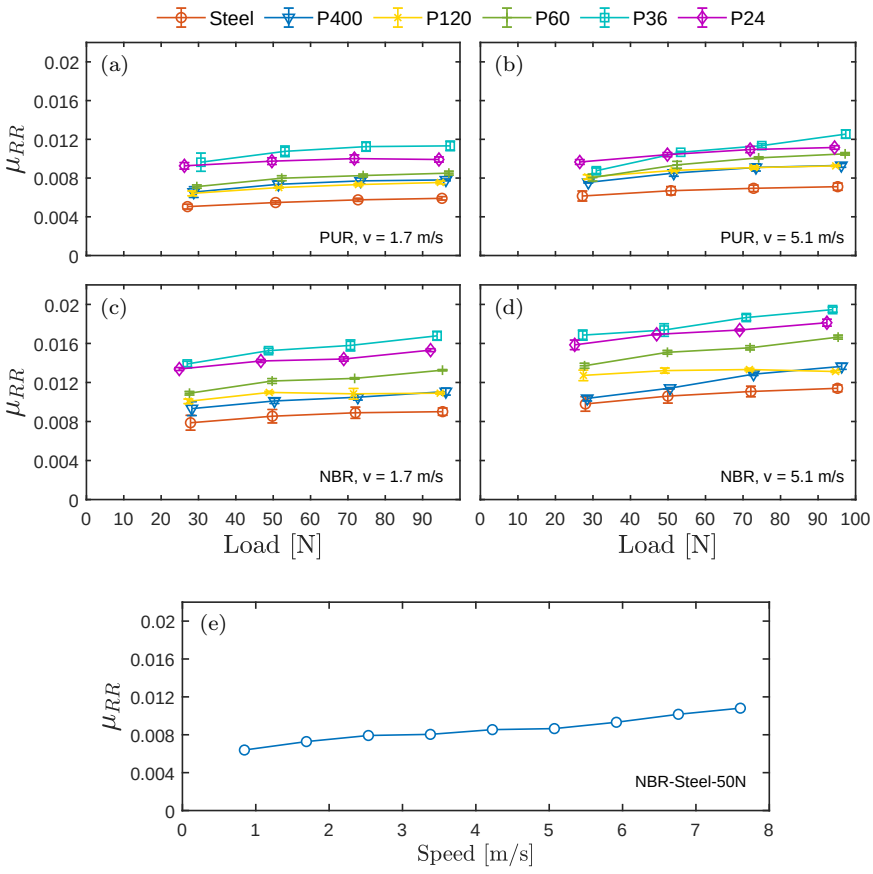

Fig. 9. Rolling resistance coefficients. (a)–(d) As a function of load and surface texture for the PUR and NBR wheels at a speed of 1.7 m/s and 5.1 m/s. (e) As a function of speed. Data are from a separate measurement run for a single load and several speeds. The trend is a weak increase with speed.

resistance coefficient with load for all studied surface textures. This could be due to the fact that we measure at quite small loads and that the curves saturate at higher loads. (4) There is a clear increase in the rolling-resistance coefficient with increasing roughness for both wheels and both studied velocities. Note that the P36 sandpaper results lie consistently above P24, which should have a coarser texture. However, the MPD value found for the P36 was higher than the that of P24, so in Fig. 10 μ_{RR} is plotted against the MPD value for a fixed load and velocity. The trend is an increase of the rolling-resistance coefficient. The data points are not monotonously increasing, though, which indicates — especially given the accuracy of the results — that the MPD measured values do not capture the essential properties of the surface texture for rolling resistance. Note that the two wheels show nearly identical behavior in this plot, only shifted slightly in the absolute level of

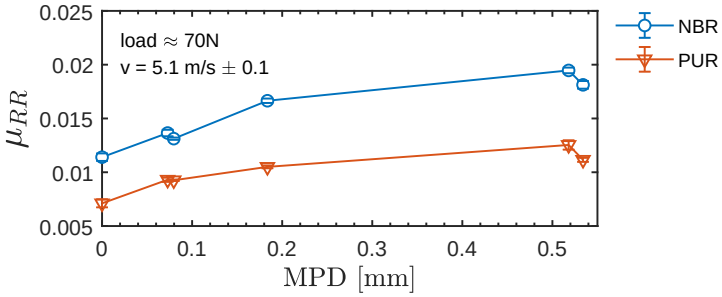

Fig. 10. Rolling resistance coefficient measurements as a function of the MPD-values. NBR and PUR wheels at a load of 70 N.

the rolling-resistance coefficient, emphasizing that the ordering of the textures is not coincidental.

3. Rolling-Resistance Modeling

For the sake of illustrating the purpose of the experimental approach, rolling-resistance calculations based on a contact model implemented with the specific dimensions and surface textures used in the experiment were performed. The contact model is based on a 3D time-dependent approach developed by Yin *et al.* [2015] for the rolling of a rigid body on a visco-elastic half-space. This configuration can be considered equivalent to the rolling of a visco-elastic solid on a rigid surface, as mentioned by Koumi *et al.* [2015] using a similar modeling approach. Only vertical stresses are considered in this study and the effect of friction on the rolling resistance is neglected. This is reasonable since it was shown by Zéhil and Gavin [2013] that the contribution of friction to rolling resistance does not exceed a few percent, implying that it can be neglected in many engineering applications.

Other rolling resistance models would have been equally relevant to study, e.g., a Finite Element Method (FEM) approach. All approaches have advantages and drawbacks: The FEM approach can model the real configuration of the setup, including complex materials and the energy dissipation due to the vibration of the wheel, but will be limited for modeling the visco-elastic contact with the surface texture, especially at smaller texture wavelengths. This may be conceivable with a more sophisticated approach based on a waveguide FEM (e.g. Hoever and Kropp [2015]). Numerical models based on the half-space assumption have been found to be relevant to predict tire/road contact in rolling conditions (e.g. Wullens and Kropp [2004] and Dubois *et al.* [2013]), taking into account surface texture at small wavelengths. In Zhang [2016], the visco-elasticity of the half-space was introduced using the approach of Yin *et al.* [2015] and this model was in good agreement with the experimental results of Zhang *et al.* [2017] in the case of a pneumatic tire rolling on a single asperity. Therefore, the approach of Yin *et al.* [2015] was used in this

study as it already proved to be relevant for modeling rolling contact of rubber-like material, including the visco-elasticity and the road surface texture.

3.1. *Calculations for test rig configurations*

The configuration introduced Yin *et al.* leads to an asymmetric final pressure distribution in the rolling direction (x-axis) when steady-state rolling is reached. This is due to energy dissipation originating from visco-elasticity, which is maximal when $v\tau_\varphi/a_0 = 1$, with $a_0 = \sqrt{r\delta}$ the radius of the contact area in the elastic case, v the rolling speed and τ_φ the characteristic creep time of the the tire material. For the purpose of this study, the rolling resistance coefficient μ_{RR} is defined as

$$\mu_{\mathrm{RR}}(t) = -\frac{M_y(t)}{P(t)r} \tag{9}$$

where r is the radius of the rolling solid, $P(t)$ is the total charge imposed and $M_y(t)$ is the resulting moment of contact stresses

$$M_y(t) = -\int_{\Sigma_c(t)} xp(x,y,t)dxdy \tag{10}$$

Note that since M_y is equal to $-\tau_{\mathrm{RR}}$ (Eq. (1)) and the time average of $P(t)$ is equivalent to F_N in the experimental section, Eq. (9) is equivalent to Eq. (8).

The contact model was run considering the NBR solid wheel configuration of the test rig. The NBR layer was assumed to be an incompressible material, leading to $\nu = 0.5$. The problem was first studied in statics for an elastic material with $E = 2.76\,\mathrm{MPa}$, i.e., $G = 0.92\,\mathrm{MPa}$. Then rolling conditions, were considered and the visco-elastic behavior of the solid wheel was approached by a standard linear visco-elastic Kelvin–Voigt model

$$\varphi(t) = \frac{1}{B_\infty} + \left(\frac{1}{B_0} - \frac{1}{B_\infty}\right) e^{-\frac{t}{\tau_\varphi}} \tag{11}$$

with $B_\infty = 1.84\,\mathrm{MPa}$, $B_0/B_\infty = 1.6$ and $\tau_\varphi = 4.56 \cdot 10^{-4}\,\mathrm{s}$. The value of B_∞ was derived through the rubber shore type A hardness value given by the supplier data sheet using empirical results from Gent [1958], while in the absence of material data the values of B_0/B_∞ and τ_ϕ were adjusted to best match the experimental results from Hansen and Larsen [2017] in the case of the NBR wheel rolling on a flat surface over normal load ranging between 25 N and 150 N and rolling speeds of 1.7 m/s and 5.1 m/s.

3.1.1. *Contact analysis in static loading conditions*

For contact analysis in static loading conditions, a potential contact area of dimensions $L_x = 25\,\mathrm{mm}$ in the longitudinal direction and $L_y = 50\,\mathrm{mm}$ in the transverse direction was considered. The spatial resolution of the mesh was $h_x = h_y = 0.5\,\mathrm{mm}$.

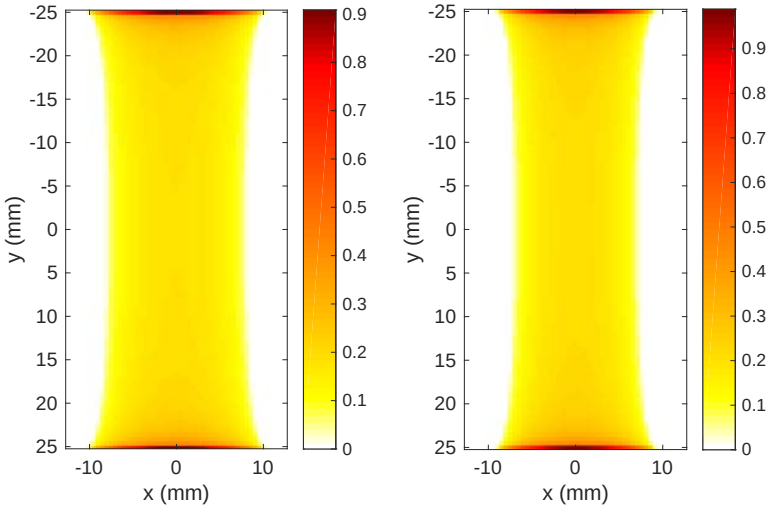

Fig. 11. Static contact pressure distribution p (in MPa) for the solid wheel in contact with the curved drum (left) and with an ideal perfectly flat surface (right) for a total load P of 150 N.

Figure 11 gives the contact pressure distribution obtained for a total load of 150 N for the elastic wheel in contact with the curved drum (left) and with a perfectly flat surface (right). While the contact prints are similar (maxima at the edges of the wheel, symmetry with respect to both axis), it is observed that the dimension of the contact area in the rolling direction is higher by about 12% in the case of the wheel in contact with the curved drum. This is purely due to geometrical conditions but can be interpreted as a higher contact stiffness in the case of the solid wheel in contact with the perfectly flat surface. However, it is assumed that this difference will have a small effect on the asymmetry of the contact pressure distribution along the longitudinal direction, which is at the origin of energy dissipation during rolling. Therefore, the drum curvature will be neglected in the following for rolling contact calculation.

In the case of rough contact, the measured 3D texture in Fig. 5 was interpolated on the mesh grid defining the surface of the solid wheel (i.e., $h_x = h_y = 0.5\,\text{mm}$). Figure 12 gives the contact pressure distribution obtained in statics for a total load of 150 N in the case of the solid wheel loaded on sandpapers P24 (left) and P60 (right). Contact pressure is distributed over surface asperities and is no longer continuous, leading to a significant decrease of the total contact area in comparison with the perfectly flat case (Fig. 11). Contact pressure peaks at the edges of the cylinders are almost removed in the presence of surface roughness, while symmetry of the contact patch disappears. Due to contact concentration on local asperities, the rougher the surface, the higher is the maximum contact pressure.

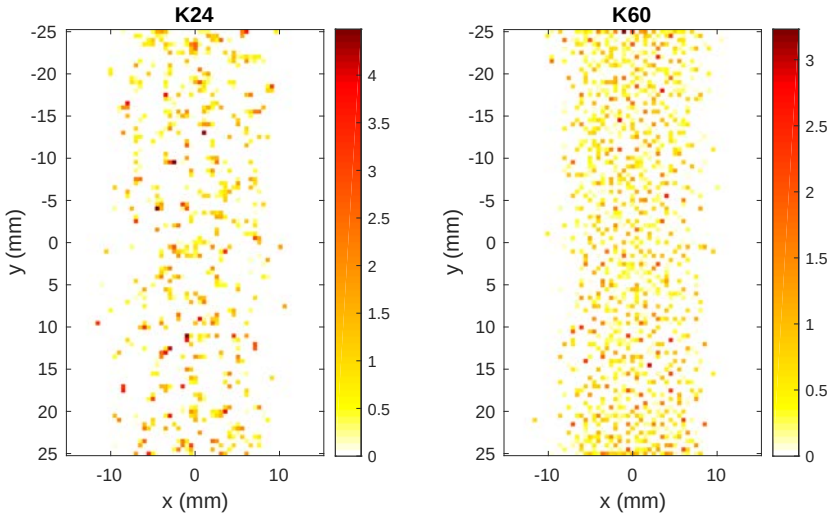

Fig. 12. Static contact pressure distribution p (in MPa) for the solid wheel in contact with sandpapers P24 (left) and P60 (right) for a total load P of 150 N.

3.1.2. *Contact analysis in rolling conditions*

For rolling contact calculation, the surface of the wheel was meshed with $h_x = 0.5\,\text{mm}$ and $h_y = 2.5\,\text{mm}$. Preliminary calculations with a finer mesh along the transverse direction y turned out to have a small influence on the rolling resistance coefficient, while increasing drastically calculation time. In the case of rough surfaces, the measured texture in Fig. 5 was downsampled by a factor of 20 and periodised to get a longer surface in the rolling direction. This is illustrated in Fig. 13

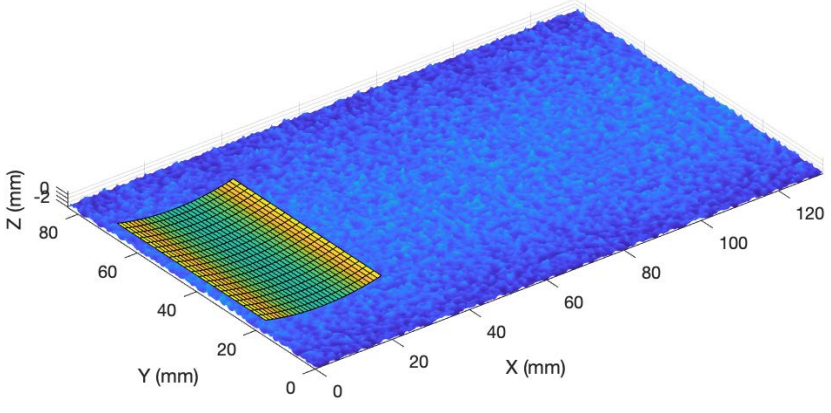

Fig. 13. Periodisation of the measured rough surface P24 for contact calculation with the solid wheel in rolling conditions.

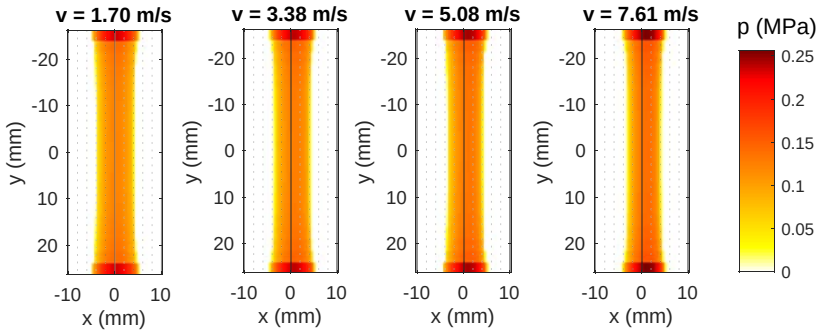

Fig. 14. Final contact pressure distribution at $t = T$ for different rolling speeds v and a total load P of 50 N in the case of the solid wheel rolling on a flat surface.

for sandpaper P24, together with the mesh of the solid wheel. During rolling the periodised rough surface was interpolated on the mesh grid of the solid wheel at each time step.

A parametric study has been performed for several values of the normal load P and the rolling speed v, which were kept constant during time. P ranged between 25 N and 150 N, while v was linearly spaced between 0.85 m/s and 7.61 m/s. In the case of the solid wheel rolling on a flat surface, Fig. 14 gives the contact pressure distribution obtained at the final time step T for $P = 50$ N and different rolling speeds. The asymmetry of the contact pressure distribution with respect to the transverse axis $y = 0$ increases with rolling speed. The higher the rolling speed, the higher is the contact pressure distribution shift to the front of the contact area. The pressure values also increase with rolling speed.

The rolling-resistance coefficient μ_{RR} as a function of time t is depicted in Fig. 15(a) for each rolling speed and a fixed total load of 50 N. The shape of the time signal is similar, but the slope at the origin increases with rolling speed. Figure 15(b) gives $\mu_{\mathrm{RR}}(t)$, and for different total load and a fixed rolling speed $v = 5.07$ m/s. In all cases, steady state is reached and μ_{RR} maintains a constant value.

In the case of rolling on sandpapers P24 and P60, Fig. 16 gives $\mu_{\mathrm{RR}}(t)$ for each total load and a constant rolling speed $v = 5.07$ m/s. Contrary to the rolling on a smooth surface (Fig. 15), the rolling-resistance coefficient does not reach a stationary state, but fluctuates slightly even during steady-state rolling conditions. While the shape of the time signals looks similar, the extreme values of the signals are slightly shifted in time, depending on the value of the vertical load.

The averaged coefficient of rolling resistance $\overline{\mu}_{\mathrm{RR}}$ as a function of the total load P is given in Fig. 17(a) for sandpapers P24 and P60. The final value of the rolling resistance coefficient $\mu_{\mathrm{RR}}(T)$ on the smooth surface is also given for comparison. Two rolling speeds of 5.07 m/s and 1.69 m/s are considered. The effect of the load and surface roughness on rolling resistance is minor for a rolling speed of 1.69 m/s.

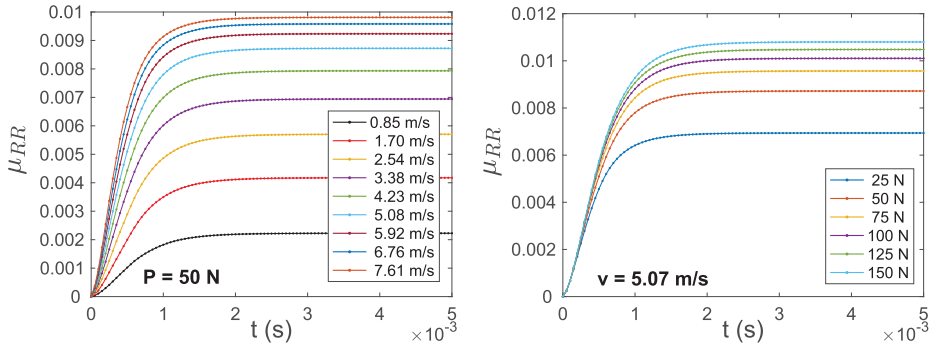

(a) (b)

Fig. 15. Rolling-resistance coefficient μ_{RR} as a function of time t for a solid wheel rolling on a flat surface. (a) For different rolling speeds v and a fixed total load $P = 50\,\mathrm{N}$. (b) For different total loads P and a fixed rolling speed $v = 5.07\,\mathrm{m/s}$.

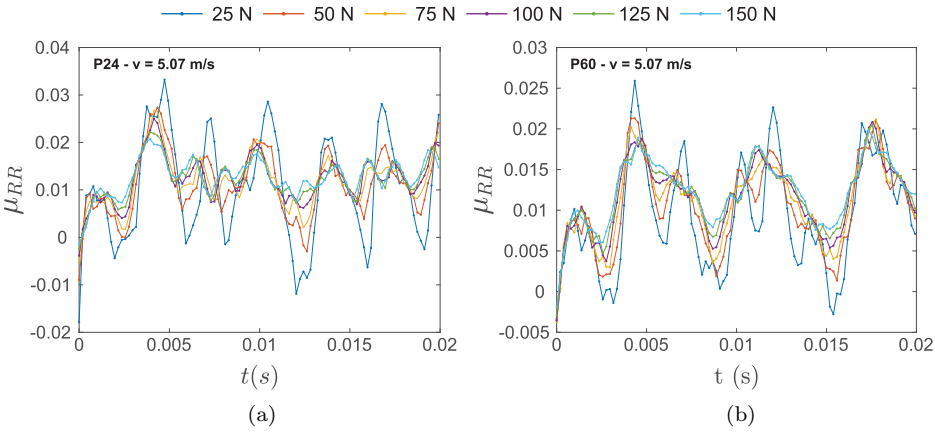

(a) (b)

Fig. 16. Rolling resistance coefficient μ_{RR} as a function of time t when the solid wheel rolls on sandpapers P24 (a) and P60 (b). The vertical load P is constant during rolling and ranges between 25 N and 150 N. The rolling speed is $v = 5.07\,\mathrm{m/s}$.

On the contrary, at the rolling speed 5.07 m/s, the averaged coefficient of rolling resistance increases with vertical load and with surface roughness.

Similarly, Fig. 17(b) gives $\overline{\mu}_{\mathrm{RR}}$ on sandpapers P24 and P60 and $\mu_{\mathrm{RR}}(T)$ on the smooth surface as a function of the rolling speed v. The total load P is fixed to 50 N. It is observed that the coefficient of rolling resistance increases with rolling speed following a nonlinear relationship for all three surfaces. At low rolling speeds, the three curves are nearly identical, while they separate out at higher rolling speeds with the P24 giving the highest rolling resistance coefficient and the flat surface the lowest.

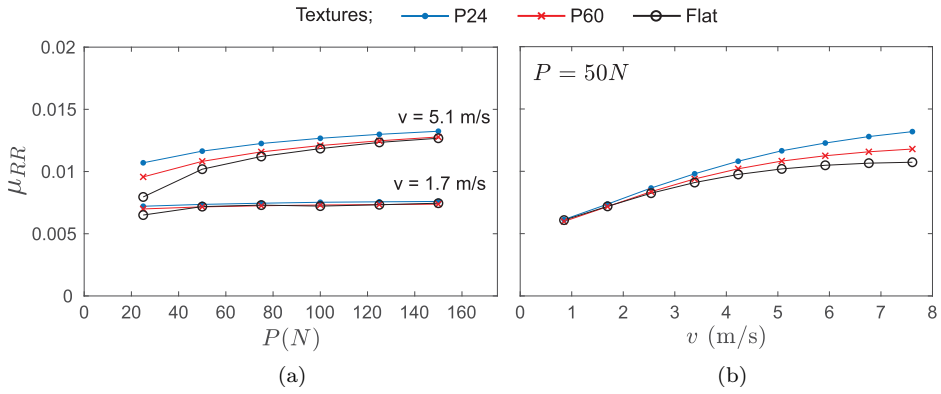

Fig. 17. Averaged coefficient of rolling resistance $\overline{\mu}_{\mathrm{RR}}$ for sandpapers P24 and P60 compared to the final rolling resistance coefficient $\mu_{\mathrm{RR}}(T)$ on the smooth surface as a function of the total normal load P for two different rolling speeds: 5.07 m/s and 1.69 m/s (a) and as a function of rolling speed, v, for $P = 50$ N (b).

4. Discussion and Concluding Remarks

4.1. *Model vs experiment*

Numerical model calculations were carried out for a solid rubber wheel on a subset of surfaces used in the experiment (smooth steel, P60 and P24), for the same rolling speeds and the same range of vertical loads, allowing for not only a qualitative comparison but also a quantitative comparison. The visco-elastic behavior of the nitril butadiene rubber used in the experiment was modeled by a Kelvin–Voigt model with three parameters: the short-time and long-time constants (respectively B_0 and B_∞) and the characteristic time, τ_ϕ.

Table 1 shows numerical and experimental values for the rolling-resistance coefficient of the NBR wheel at a load of 50 N. The values are similar in magnitude and nearly identical for the flat (smooth steel) surface the values, which is not surprising since the visco-elastic parameters for the rubber model were adjusted to these conditions. The experimental values are consistently higher for the textured surfaces. The increase in the rolling resistance coefficient with surface roughness is larger in the experimental data, while the relative increase with speed for a given surface is

Table 1. Comparison of measured and predicted rolling resistance coefficient at $P = 50$ N for two rolling speeds $v = 1.7$ m/s and $v = 5.1$ m/s in the case of the NBR solid wheel.

v	1.7 m/s		5.1 m/s	
	Experimental	Numerical	Experimental	Numerical
Flat	0.0085	0.0072	0.0106	0.0102
P60	0.0122	0.0072	0.0132	0.0108
P24	0.0142	0.0074	0.0169	0.0116

larger for the numerical results. The numerical results are nearly independent of surface texture studied here at the low speed.

Generally, a higher value for experimental measurements compared to numerical values is not unexpected, given that not all effects (e.g., vibrational losses) are considered in the model. The difference for textured surfaces is, on the other hand, dramatic and might indicate unknown sources of error, either in the model or the experiment. In the experiment, one additional source of loss could be the layer of double sided tape that fixates the sandpaper in the drum. This is, however, a very thin layer so this would most likely be a minor contribution.

Another more likely possibility for the deviations is the model for the viscoelastic properties of the rubber not being accurate enough. An obvious improvement would be to measure the complex frequency-dependent shear modulus of the rubber by a different technique and to fit a generalized Kelvin model to the measured creep function instead of using the Kelvin–Voigt model with a single creep characteristic time. It is likely that some characteristic times missing in the present model will dissipate energy at smaller length scale than the contact patch length in the rolling direction, e.g., at the scale of characteristic asperity sizes present for rough surfaces. This could partly explain the underestimation of rolling resistance observed in this study with the model in the case of rough surface in comparison with experimental results.

4.2. *Our experiment vs other experiments*

As discussed in the introduction, the approach of scaling down the experimental setup and working with solid wheels — instead of pneumatic tires in full scale measurements — is not very common, especially combined with the primary purpose being the test and validation of models for rolling resistance. A study by Lundberg *et al.* [2017] has a similar idea of constructing a test rig for controlled measurements of contact forces. Their focus, however, is complementary to ours, namely delivering reliable empirical input for tire construction in the absence of a theoretical understanding where we aim for a reliable model-validation setup.

Riahi *et al.* [2020] reported another simplified setup to measure texture-dependent rolling resistance. They use a Wehner/Schulze polishing machine containing three rubber cones mounted on the rotary head and rolling on a given road specimen. The focus here was on how to relate (or translate) these faster and simpler measurements to trailer measurements on the same road surfaces.

Pneumatic tires are complicated structures with many layers of different materials, tread patterns, etc. This makes direct comparisons with full scale measurements of rolling-resistance coefficient — either on drums or on actual roads — less obvious. Yet, the values obtained in this work (both for model and experiment) are in the same range as those typically obtained in full scale measurements, $\mu_{\mathrm{RR}} = 0.005$–$0.02$ [Anfosso-Lédée *et al.*, 2016; Bergiers *et al.*, 2011; Ejsmont *et al.*, 2016], indicating that the main contribution to the rolling resistance loss is the rubber, also in the

pneumatic tires. Comparing trends in our experiment with full scale measurements might therefore still be relevant.

We found the rolling-resistance coefficient to depend on all the controlled parameters: load, speed, surface texture and wheel material type. To start with the latter, it is hardly surprising that the material influences the loss. The frequency-dependent visco-elastic properties of different types of elastomers are known to be different and also to vary with molecular weight, filler content, etc. within the same type [Ferry, 1980]. Thus, the overall magnitude of the rolling-resistance coefficient as well as rolling speed dependence should be different, especially in the simplified case of solid rubber wheel used in our experiment. We found that the rolling-resistance coefficient for the PUR wheel was consistently lower than that of the NBR wheel for a given combination of speed, load and texture. Similarly, [Benninger, 2008] showed that in a full-scale tire design based on polyurethane instead of natural rubber, the rolling resistance in the lab under identical conditions was significantly (about a factor of 2) lower. Also, the rolling-resistance coefficient for the PUR wheel showed only a weak speed dependence, which indicates that at ambient conditions, the typical time scale for visco-elastic response of the PUR is higher, leading to a more elastic, yet slightly increasing, speed-dependent behavior. The loss could also be generally lower in polyurethane compared to the nitrile butadiene rubber.

Various publications report the rolling resistance be independent of, or even decreasing, with the speed. The speeds in these studies are normal driving speeds, i.e., between 50 km/hand 80 km/h corresponding to 13.9 m/s and 22.2 m/s and thus — if the rolling resistance in car tires is mostly due to visco-elastic effects in the tire rubber — they could be due to the "deformation frequency" being on the high-frequency side of the mechanical loss peak.

The mere definition of the rolling-resistance coefficients given in Eq. (8) assumes the rolling-resistance force to depend linearly on the load, i.e., the rolling-resistance coefficient to be *independent* of the load. We found it be weakly, but consistently, increasing with load for both wheels on all tested surfaces and tested rolling speeds. The rate of increase is for some measurements decreasing, and thus the curves may approach a plateau where μ_{RR} is constant. Some full scale studies showing rolling-resistance coefficients to be independent of load within the error of the measurement (see, e.g., Bergiers *et al.* [2011]) might therefore be due to a somewhat higher load being used in those experiments. On the other hand, Ejsmont *et al.* found both increasing, decreasing and constant rolling resistance coefficients as a function of load, so the specific load dependence appears to depend on the exact details of the test tire.

4.3. *Texture measures*

A road surface is complicated with structure on many length scales [Sandberg *et al.*, 2011; Quan *et al.*, 2013; Andersen *et al.*, 2015], so one of the important questions is what parameters are essential for characterizing the roughness to predict the

resulting rolling resistance. Some works claim that the MPD measure [Delanne, 1994; Sandberg *et al.*, 2011] or the RMS texture depth Lopez [2010] is a good predictor of rolling resistance. Others point in the direction that enveloping effects need to be taken into account [Pinnington, 2012; Andersen, 2015; Ejsmont *et al.*, 2016; Goubert and Sandberg, 2018; Vieira *et al.*, 2019]. This makes sense, since the tire does not necessarily "see" the bottom of the texture, but definitely the top. This is also supported by Kawakami *et al.* [2017] who found that the distribution of contact pressure between tire and pavement surface provides a better correlation with the rolling-resistance coefficient.

In this study, six surface textures were investigated: P24, P36, P60, P120, P400 and steel. The steel surface is assumed to have a MPD value of practically zero. Categorizing the sandpaper using a profilometer to calculate MPD values gave nearly the same ordering as suggested by the grit size, except for P36 that turned out to have a higher MPD value than P24. At first this may seem surprising, since P24 should be coarser than the P36, but the grit size only gives the number of grits per area which does not necessarily imply anything about the depth of the texture. Normally, these quantities scale with each other, which could explain why in some studies a good correlation with MPD is found. In Figs. 9 and 10, the general tendency is an increasing μ_{RR} with increasing MPD value, though not monotonically within the accuracy of the measurement, suggesting that the MPD is a too simple measure and that a measure including more details of the texture (as the self-affine measure suggested by Torbruegge and Wies [2015]) or including only the part of the texture that the tire sees (as the MPD combined with some enveloping function suggested by Goubert and Sandberg [2018] and Ejsmont and Sommer [2021]) is more appropriate.

In a continuation of this work, we aim to use 3D printed surfaces for absolute control over the texture. In this way, one can critically test possible correlations of texture measures with the measured rolling resistance.

5. Summary

This paper described a setup for the validation of rolling-resistance models under controlled circumstances. The fundamental idea is that, if one has a valid quantitative model for the rolling resistance between tire and road, this model must also work for solid wheels rolling on sandpaper.

We carried out a systematic parametric study of the rolling-resistance coefficient with our scaled-down drum setup that accurately measures the rolling resistance of solid rubber wheels. The rolling-resistance coefficient increases with increasing rolling speed and increasing load and depends on the rubber type and surface roughness. These results were compared to numerical calculations adjusted to replicate the experimental setup in dimensions, materials and surfaces. The numerical results agree qualitatively with the experimental results, but lack a complete quantitative

agreement, in general predicting a lower rolling-resistance coefficient than what is found experimentally. This shows that the model could be improved, e.g., by a proper characterization of the visco-elastic properties of the rubber. We conclude that the approach demonstrates the usefulness of having a rolling-resistance model validation laboratory that simplifies the experiment to obtain a high degree of control.

Acknowledgments

A special thanks goes the Danish Road Directorate for helping with profilometer measurements of textures.

This work was supported by the VILLUM Foundation's Matter (Grant No. 16515), Innovation Fund Denmark as a part of the ROSE Project (No. 5160-00009B), and the Danish Road Directorate.

References

Andersen, L. G., Larsen, J. K., Fraser, E. S., Schmidt, B. and Dyre, J. C. [2015] "Rolling resistance measurement and model development," *Journal of Transportation Engineering* **141**(2), doi:10.1061/(ASCE)TE.1943-5436.0000673.

Andersen, L. G. [2015] "Rolling resistance modelling: From functional data analysis to asset management system," PhD thesis, Roskilde University, Roskilde, Denmark.

Anfosso-Lédée, F., Cerezo, V., Karlsson, R., Bergiers, A., Dauvergne, S., Ejsmont, J., Goubert, L., Lesdos, H., Maeck, J., Sandberg, U., Sjogren, L. and Zller, M. [2016] "Experimental validation of the rolling resistance measurement method including updated draft standard," Resreport, IFSTTAR, ROSANNE Deliverable D3.6.

Araújo, J. P. C., Palha, C. A., Martins, F. F., Silva, H. M. and Oliveira, J. R. [2019] "Estimation of energy consumption on the tire-pavement interaction for asphalt mixtures with different surface properties using data mining techniques," *Transportation Research Part D: Transport and Environment* **67**, 421, doi:10.1016/j.trd.2018.12.022.

Bazi, G., Hajj, E. Y., Ulloa-Calderon, A. and Ullidtz, P. [2018] "Finite element modelling of the rolling resistance due to pavement deformation," *International Journal of Pavement Engineering* **21**(3), 365–375, doi:10.1080/10298436.2018.1480778.

Benninger, G. N. [2008] "A status report on the Amerityre pneumatic polyurethane passenger car tire," Techreport, Amerityre Corporation, https://www.rubbernews.com/assets/PDF/RN86184218.pdf.

Bergiers, A., Goubert, L., Anfosso-Lédée, F., Dujardin, N., Ejsmont, J. A., Sandberg, U. and Zöller, M. [2011] "Comparison of rolling resistance measuring equipment — pilot study," Resreport, VTI, MIRIAM, SP1 Deliverable No. 3.

Boere, S., Arteaga, I. L., Kuijpers, A. and Nijmeijer, H. [2014] "Tyre/road interaction model for the prediction of road texture influence on rolling resistance," *International Journal of Vehicle Design* **65**(2/3), 202, doi:10.1504/IJVD.2014.060815.

Chupin, O., Piau, J.-M. and Chabot, A. [2013] "Evaluation of the Structure-induced Rolling Resistance (SRR) for pavements including viscoelastic material layers," *Materials and Structures* **46**(4), 683–696, doi:10.1617/s11527-012-9925-z.

Delanne, Y. [1994] "The influence of pavement evenness and macrotexture on fuel consumption," in *Vehicle-Road Interaction*, ed. B. Kulakowski (ASTM International, West Conshohocken), doi:10.1520/STP13259S.

Dubois, G., Cesbron, J., Yin, H. P., Anfosso-Lédée, F. and Duhamel, D. [2013] "Statistical estimation of low frequency tyre/road noise from numerical contact forces," *Applied Acoustics* **74**(9), 1085–1093.

Ejsmont, J., Taryma, S., Ronowski, G. and Swieczko-Zurek, B. [2016] "Influence of load and inflation pressure on the tyre rolling resistance," *International Journal of Automotive Technology* **17**(2), 237–244, doi:10.1007/s12239-016-0023-z.

Ejsmont, J. A., Ronowski, G., Świeczko Żurek, B. and Sommer, S. [2017] "Road texture influence on tyre rolling resistance," *Road Materials and Pavement Design* **18**(1), 181–198, doi:10.1080/14680629.2016.1160835.

Ejsmont, J. and Owczarzak, W. [2019] "Engineering method of tire rolling resistance evaluation," *Measurement* **145**, 144–149, doi:10.1016/j.measurement.2019.05.071.

Ejsmont, J. and Sommer, S. [2021] "Selected aspects of pavement texture influence on tire rolling resistance," *Coatings* **11**(7), 776, doi:10.3390/coatings11070776.

Ferry, J. D. [1980] *Viscoelastic Properties of Polymers* (John Wiley & Sons, Brisbane, Queensland, Australia), pp. 1–12.

Gent, A. N. [1958] "On the relation between indentation hardness and Young's Modulus," *Rubber Chemistry and Technology* **31**(4), 896–906, doi:10.5254/1.3542351.

Goubert, L. and Sandberg, U. [2018] "Enveloping texture profiles for better modelling of the rolling resistance and acoustic qualities of road pavements," *8th Symposium on Pavement Surface Characteristics*: *SURF* 2018 — *Vehicle to Road Connectivity*, Australian Road Research Board (ARRB).

Haider, M., Conter, M., Green, M., Schmidt, B. and Sandberg, U. [2016] "Status of the eu-project ROSANNE," *Transportation Research Procedia* **14**, 2946–2955, doi:doi:10.1016/j.trpro.2016.05.415.

Hansen, L. and Larsen, M. [2017] An experimental investigation of rolling resistance, Master's thesis, Roskilde University.

Hoever, C. and Kropp, W. [2015] "A model for investigating the influence of road surface texture and tyre tread pattern on rolling resistance," *Journal of Sound and Vibration* **351**, 161–176, doi:10.1016/j.jsv.2015.04.009.

ISO13473 [2019] "Characterization of pavement texture by use of surface profiles — part 1: Determination of mean profile depth," Standard ISO 13473-1:2019, International Organization for Standardization, Geneva, CH, https://www.iso.org/standard/45111.html.

ISO18164 [2005] "Passenger car, truck, bus and motorcycle tyres — methods of measuring rolling resistance," Standard ISO 18164:2005, International Organization for Standardization, Geneva, CH, https://www.iso.org/standard/33328.html.

ISO25280 [2018] "Passenger car, truck and bus tyres — methods of measuring rolling resistance — single point test and correlation of measurement results," Standard ISO 28580:2018, International Organization for Standardization, Geneva, CH, https://www.iso.org/standard/67531.html.

Kawakami, A., Ishigaki, T., Shirai, Y., Terada, M. and Kubo, K. [2017] "Evaluation method of pavement surface characteristics for rolling resistance," *Road Materials and Pavement Design* **18**(Suppl. 2), 2–11, doi:10.1080/14680629.2017.1304264.

Kim, S.-J. and Savkoor, A. R. [1997] "The contact problem of in-plane rolling of tires on a flat road," *Vehicle System Dynamics* **27**(Suppl. 001), 189–206, doi:10.1080/00423119708969654.

Koumi, K. E., Chaise, T. and Nelias, D. [2015] "Rolling contact of a rigid sphere/sliding of a spherical indenter upon a viscoelastic half-space containing an ellipsoidal inhomogeneity," *Journal of the Mechanics and Physics of Solids* **80**, 1–25, doi:10.1016/j.jmps.2015.04.001.

Lin, Y.-J. and Hwang, S.-J. [2004] "Temperature prediction of rolling tires by computer simulation," *Mathematics and Computers in Simulation* **67**(3), 235–249, doi:10.1016/j.matcom.2004.07.002.

Lopez, I. [2010] "Influence of material damping on the prediction of road texture and tread pattern related rolling resistance," *Proceeding of ISMA 2010*, Leuven, Belgium, 4039–4052.

Lundberg, O. E., Kari, L. and Arteaga, I. L. [2017] "A compact internal drum test rig for measurements of rolling contact forces between a single tread block and a substrate," *Measurement* **103**, 370 – 378, doi:10.1016/j.measurement.2016.12.041.

Mansura, D. A., Thom, N. H. and Beckedahl, H. J. [2018] "Numerical and experimental predictions of texture-related influences on rolling resistance," *Transportation Research Record: Journal of the Transportation Research Board* **2672**(40), 430–439, doi:10.1177/0361198118776114.

Miège, A. J. P. and Popov, A. A. [2005] "Truck tyre modelling for rolling resistance calculations under a dynamic vertical load," *Proceedings of the Institution of Mechanical Engineers, Part D: Journal of Automobile Engineering* **219**(4), 441–456, doi:10.1243/095440705X11176.

Narasimha Rao, K. V., Kumar, R. K. and Bohara, P. C. [2006] "A sensitivity analysis of design attributes and operating conditions on tyre operating temperatures and rolling resistance using finite element analysis," *Proceedings of the Institution of Mechanical Engineers, Part D: Journal of Automobile Engineering* **220**(5), 501–517, doi:10.1243/09544070JAUTO170.

Nielsen, N. R., Chatti, K., Nielsen, C. P., Zaabar, I., Hjorth, P. G. and Hecksher, T. [2020] "Method for direct measurement of structural rolling resistance for heavy vehicles," *Transportation Research Record* **2674**(5), 371–380, doi:10.1177/0361198120915699.

Park, H. C., Youn, S., Song, T. S. and Kim, N. [1997] "Analysis of temperature distribution in a rolling tire due to strain energy dissipation," *Tire Science and Technology* **25**(3), 214–228, doi:10.2346/1.2137541.

Pinnington, R. J. [2012] "A particle-envelope surface model for roadtyre interaction," *International Journal of Solids and Structures* **49**(3), 546–555, doi:10.1016/j.ijsolstr.2011.10.022.

Pouget, S., Sauzéat, C., Benedetto, H. D. and Olard, F. [2012] "Viscous energy dissipation in asphalt pavement structures and implication for vehicle fuel consumption," *Journal of Materials in Civil Engineering* **24**(5), 568–576, doi:10.1061/(ASCE)MT.1943-5533.0000414.

Quan, W., Wang, H., Liu, X. and Zhang, S. [2013] "Multi-fractal analysis for pavement roughness evaluation," *Procedia - Social and Behavioral Sciences* **96**, 2684–2691, doi:10.1016/j.sbspro.2013.08.301.

Riahi, E., Ropert, C. and Do, M.-T. [2020] "Developing a laboratory test method for rolling resistance characterisation of road surface texture," *Surface Topography-Metrology and Properties* **8**(2), 024006, doi:10.1088/2051-672X/ab8aa6.

Sandberg, U., Bergiers, A., Ejsmont, J. A., Goubert, L., Karlsson, R. and Zöller, M. [2011] "Road surface influence on tyre/road rolling resistance," Resreport, VTI, MIRIAM, SP1 Deliverable No. 4.

Sandberg, U., Haider, M., Conter, M., Goubert, L., Bergiers, A., Glaeser, K.-P., Schwalbe, G., Zöller, M., Boujard, O., Hammarström, U., Karlsson, R., Ejsmont, J. A., Wang,

T. and Harvey, J. [2015] "Rolling resistance – basic information and state-of-the-art on measurement methods," Resreport, VTI, MIRIAM, SP1 Deliverable No. 1.

Sharma, A. K., Bouteldja, M. and Cerezo, V. [2020] "Multi-physical model for tyre — road contact — the effect of surface texture," *International Journal of Pavement Engineering* **0**(0), 1–18, doi:10.1080/10298436.2020.1769844.

Stutts, D. and Soedel, W. [1992] "A simplified dynamic model of the effect of internal damping on the rolling resistance in pneumatic tires," *Journal of Sound and Vibration* **155**(1), 153–164, doi:10.1016/0022-460X(92)90652-E.

Torbruegge, S. and Wies, B. [2015] "Characterization of pavement texture by means of height difference correlation and relation to wet skid resistance," *Journal of Traffic and Transportation Engineering* **2**(2), 59–67.

Vieira, T., Sandberg, U. and Erlingsson, S. [2019] "Negative texture, positive for the environment: Effects of horizontal grinding of asphalt pavements," *Road Materials and Pavement Design* **22**(1), 1–22, doi:10.1080/14680629.2019.1610476.

Willis, J. R., Robbins, M. M. and Thompson, M. [2015] "Effects of pavement properties on vehicular rolling resistance: A literature review," Technical Report, National Center for Asphalt Technology.

Wullens, F. and Kropp, W. [2004] "A three-dimensional contact model for tyre/road interaction in rolling conditions," *Acta Acustica* **90**, 702–711.

Yin, H. P., Cesbron, J. and Bui, Q. H. [2015] "A new formulation for solving 3D time dependent rolling contact problems of a rigid body on a viscoelastic half-space," *Mechanics Research Communications* **64**, 8–14, doi:10.1016/j.mechrescom.2014.12.006.

Zéhil, G.-P. and Gavin, H. P. [2013] "Three-dimensional boundary element formulation of an incompressible viscoelastic layer of finite thickness applied to the rolling resistance of a rigid sphere," *International Journal of Solids and Structures* **50**(6), 833–842, doi:10.1016/j.ijsolstr.2012.11.020.

Zöller, M. [2014] "State of the art on rolling resistance measurement devices," techreport, AIT, ROSANNE, Deliverable D3.1, https://www.rosanne-project.eu/documents?id=7299.

Zhang, Y.-F., Cesbron, J., Yin, H.-P. and Bérengier, M. [2017] "Experimental study of normal contact force between a rolling pneumatic tyre and a single asperity," *International Journal of Applied Mechanics* **9**(7), 1750081, doi:10.1142/S1758825117500818.

Zhang, Y. [2016] Study on a test rig of dynamic tyre/road contact forces at the origin of rolling noise, PhD thesis, cole Centrale de Nantes – Université Bretagne Loire.